RSC Advances

PAPER

View Article Online
View Journal | View Issue

Cite this: *RSC Adv.*, 2020, **10**, 27775

Thermodynamic investigation with chemical kinetic analysis on the reoxidation phenomenon of the Cr(III) in air†

Qining Liu,[ab] Honghui Liu,[ab] Huixia Chen,*[ab] Xinrun Wang,*[c] Dahai Hu,[d] Xichuan Cheng[e] and Hongbin Xu[ab]

In this paper, the reoxidation behaviours of CrOOH and $Cr(OH)_3$ are investigated as the major reduction products of Cr(VI). The atmosphere oxidation of Cr(III) is studied in the environment of soil without manganese and hydrogen peroxide. The influence of temperature and pH value on the oxidation rate of Cr(III) is examined by Experiment methods in details. According to the experimental results, the oxidation of Cr(III) is promoted in the environment with high pH value, however, the oxidation process is stable with temperature. The oxidation process of CrOOH and $Cr(OH)_3$ are theoretically researched by thermodynamic calculation and density functional theory (DFT) simulation. The results of DFT indicate that both CrOOH and $Cr(OH)_3$ are oxidized during the chemical adsorption process of O_2 in alkaline environment. With the transformation from Cr(III) to Cr(VI), the Cr–O covalent bond forms in the adsorption process. The crystal structure difference between CrOOH and $Cr(OH)_3$ leads to the different oxidation reaction between O_2 and Cr(III). The significant alteration of oxidation process in (110), (310), (321) crystal planes is also observed indicating the crystal orientation dependence. Based on the chemical reaction kinetics, the chemical equivalent constant K of CrOOH is higher than $Cr(OH)_3$, illustrating higher chemical stability in air. In summary, both experimental study and theoretical analysis on the reoxidation phenomenon of Cr(III) reduced from Cr(VI) in natural environment demonstrate that not only the external factors such as temperature and pH value but also the crystal structure of Cr(III) compound have dramatic influence on the oxidation process.

Received 13th February 2020
Accepted 13th July 2020

DOI: 10.1039/d0ra01403f

rsc.li/rsc-advances

1. Introduction

With the development of industrial production, the contamination of chromium becomes more and more serious. Most of the polluted areas are distributed in the legacy site after the migration of the old factory. The maximum level of Cr(VI) in contaminated soil setting by the US Environmental Protection Agency is 1240 ppm.[1] The maximum concentration of Cr(VI) in soil is: 100 mg kg^{-1} in Germany and 120 mg kg^{-1} in Canada.[2] However, according to the results of sampling and analysis of the surrounding soil of contaminated area *e.g.* buried field, the total chromium content of sample points can reach to the values of 581.75–7060.00 mg kg^{-1} that is far beyond the requirement of the quality control standard. As far as the existence of valence state of chromium is concerned, Cr(III) and Cr(VI) are two common aerobic states in soil. Chromium is the essential trace element of human and animal in the stable form of Cr(III), however, is highly toxic and harmful in the easy-to-migrate form of Cr(VI).[3] The feature of easy migration makes Cr(VI) not only expand the range of soil pollution, but also pollute surface water and groundwater. Nowadays, people usually use the $FeSO_4$ and Na_2S as the reduction to reduce the Cr(VI) that far above the standard. $FeSO_4$ can reduce the Cr(VI) in acidic and neutral conditions, and generate CrOOH in weak acid or neutrally condition then precipitate $Cr(OH)_3$ sediment in alkaline environment.[4,5] Na_2S can reduce Cr(VI) to Cr(III),[6] producing SO_4^{2-} (ref. 7) or S[8] as the oxidize production, and mainly producing $Cr(OH)_3 \cdot nH_2O$ in alkaline condition as the reduction of Cr(III).

CrOOH and $Cr(OH)_3$, slightly soluble in water, are usually known as the stable reduction product of Cr(III).[9] From the evaluation results of short-term remediation effect, it is found that the reduction and remediation of Cr(VI) contaminated soil

[a]*CAS Key Laboratory of Green Process and Engineering, Institute of Process Engineering, Chinese Academy of Sciences, Beijing 100190, China. E-mail: hxchen@ipe.ac.cn; Tel: +86 13426451886*

[b]*National Engineering Laboratory for Hydrometallurgical Cleaner Production Technology, Institute of Process Engineering, Chinese Academy of Sciences, Beijing 100190, China*

[c]*State Key Laboratory of Environmental Criteria and Risk Assessment, Chinese Research Academy of Environmental Sciences, Beijing 100012, China*

[d]*Yuhuan Environmental Technology Co. LTD, Shijiazhuang 050091, Hebei Province, China*

[e]*Hubei Zhenhua Chemical Co. LTD, Huangshi 435001, Hubei Province, China*

† Electronic supplementary information (ESI) available. See DOI: 10.1039/d0ra01403f

can basically reach the established standard, but there is a rebound in the concentration of Cr(VI) after reduction and restoration.[10] Researchers make two kinds of arguments about this phenomenon after reduction and treatment of the soil. Unavoidable, the detection accuracy of Cr(VI) in soil is one of defect of the reason of "Reoxidation of Cr(III)".[11,12] The second view is that Cr(III) can be oxidized by Mn and H_2O_2.[13] A large number of laboratory studies have shown that manganese oxide can oxidize Cr(III) to Cr(VI) Fandeur.[14] It can easily trigger the oxidizing reaction with strong adsorption capacity and high oxidation potential.[15] In addition, H_2O_2 is also a natural oxidant in soil environment.[16] H_2O_2 can be produced by biological metabolic process, soil weathering process and photochemical process.[15] Cr(III) can produce intermediate Cr(VI), Cr(V) and newly forming (–OH) with highly oxidation.[17]

However, no previous work has been done to study if oxygen is the contributing factor in the oxidation process of Cr(III) to Cr(VI), especially in the wet alkaline environment. Without the function of catalysis, oxygen has the possibility to become the potential oxide in theory. In this paper, we study the reoxidation of Cr(III) in the air without MnO_2 and H_2O_2. By reducing the Cr(VI) with $FeSO_4$ and Na_2S, we can get CrOOH and $Cr(OH)_3 \cdot nH_2O$ within different pH. A step further, we proceed condition experiment with Cr(III) exposed to air in different pH (6, 8, 10, 12, 14) and temperatures (20 °C, 40 °C, 60 °C, 80 °C, 100 °C). The Cr(III) samples before and after the oxidation process were characterized by SEM and XPS. Through quantitative analysis by spectrophotometric method, we can get Cr(VI) content at each 12 hours. In addition, kinetic models was used to described the oxidation process of Cr(III). Based on the thermodynamic investigation, the principle of Cr(III) oxidized to Cr(VI) could be acquired within different pH at certain temperature which is closed to the soil environment. In addition, we compute the adsorb energy of Cr(III) reacting with oxygen by DFT (density functional theory), with the results of DOS (density of state) and PDOS (partial density of state) before and after the Cr(III) reacting with oxygen.

2. Experiment and computational method

2.1 Experiment

CrOOH was prepared by the reaction of Na_2CrO_4 with $FeSO_4 \cdot 7H_2O$ (made by Aladdin company, analytically pure) in acid or neutral condition (pH = 5–7), and then filtered in alkaline

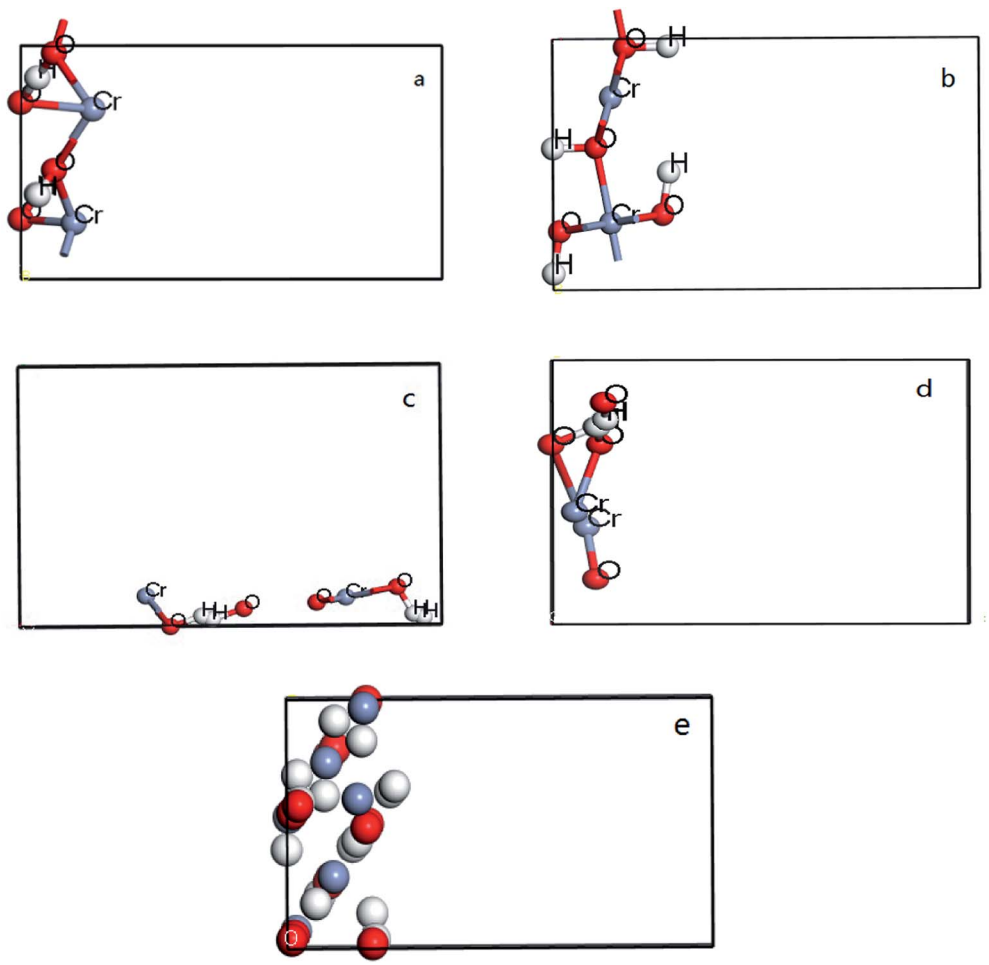

Fig. 1 (a) Vertical view from CrOOH (101) surface; (b) vertical view from CrOOH (110) surface; (c) vertical view from CrOOH (310) surface; (d) vertical view from CrOOH (321) surface; (e) vertical view from $Cr(OH)_3$.

condition (pH > 8). Meanwhile, $Cr(OH)_3$ was obtained by the reaction of Na_2CrO_4 with $Na_2S{\cdot}9H_2O$ (made by Aladdin company, analytically pure) in alkaline condition (pH > 12), and then filtered in the same condition. Thoroughly clean the CrOOH and $Cr(OH)_3$ with distilled water, and rinse completely so there is no residual Cr(VI). After the filtering process, the Cr(III) sample was dried in FD-1A-50 vacuum freeze dryer (manufactured by BIOCOOL company, vacuum value < 9 Pa) by 24 hours.

The CrOOH and $Cr(OH)_3$ were separated into four groups, studying the effects of temperature and pH on reoxidation of Cr(III) in air under different conditions. In the reoxidation process, 50 mg CrOOH and $Cr(OH)_3$ was dissolved respectively in a certain amount of deionized water. In order to contrast the temperature, the samples of Cr(III) were exposed to the air at room temperature and placed in 40 °C, 60 °C, 80 °C and 100 °C DZF-6096 oven (manufactured by Shanghai YIHENG company) respectively. In addition, the pH value of Cr(III) was buffered in the solution (pH = 6, 8, 10, 12, 14). After each of 12 hours, the hexavalent chromium concentration in the solution was analysed by ultraviolet spectrophotometer (constructed by PERKINELMER company, measuring wavelength from 190 nm–900 nm).

The microstructure, compositions and chemical bonding states of the CrOOH and $Cr(OH)_3$ were studied using scanning electron microscope (SEM), X-ray photoelectron spectroscopy (XPS). SEM analyses were performed using JSM-7001F + INCA X-MAX. The XPS measurements were performed using a Thermo Fisher ESCALAB 250 Xi instrument which equipped with a Mg Ka X-ray source (power of 300 W).

2.2 Computational method and model

All DFT calculations are performed by using CASTEP code in Materials studio 8.0. In the calculation process, the periodic

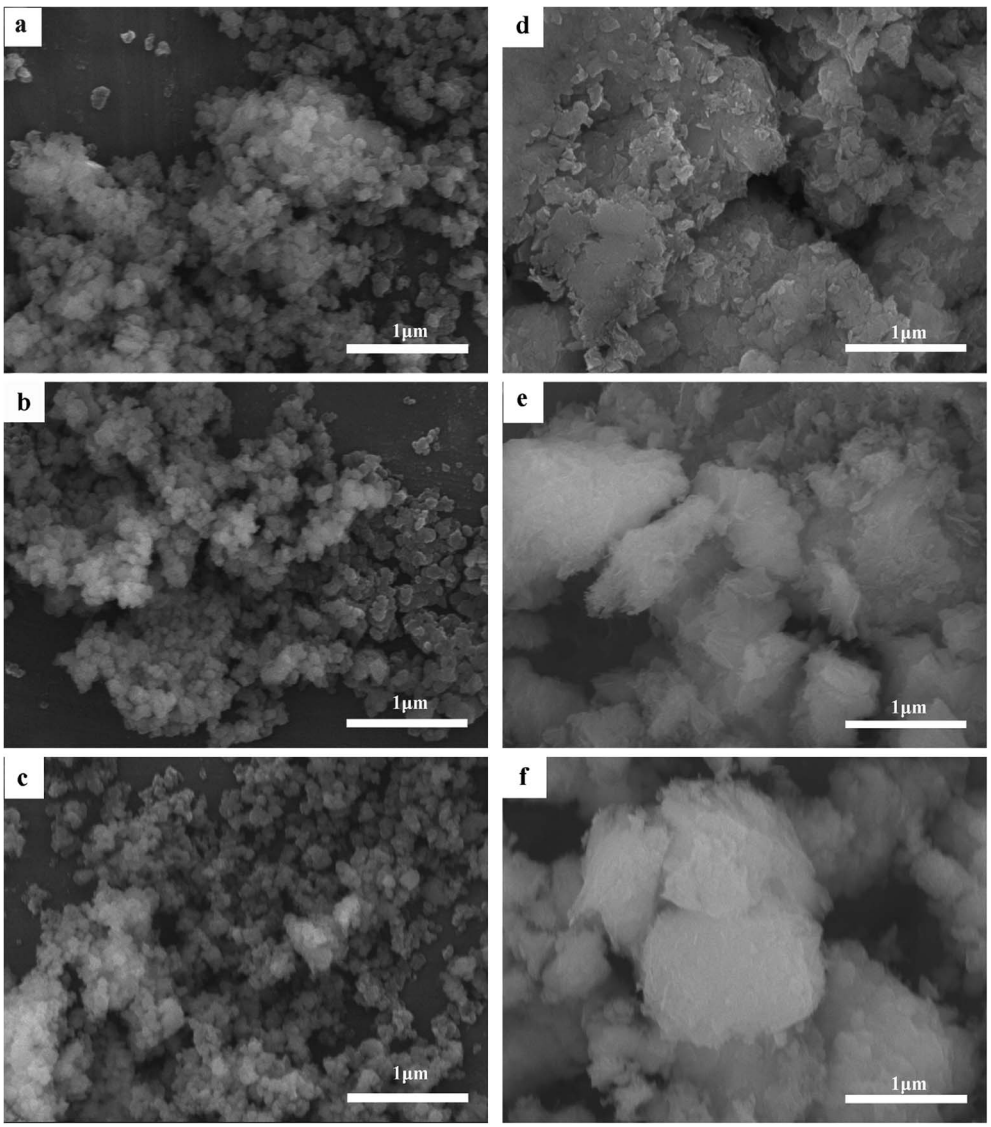

Fig. 2 Morphology of Cr(III) before and after the oxidation: (a) the $Cr(OH)_3$ original sample; (b) the $Cr(OH)_3$ at 100 °C; (c) the $Cr(OH)_3$ at pH = 14; (d) the CrOOH original sample; (e) the CrOOH at 100 °C; (f) the CrOOH at pH = 14.

boundary condition is used to replace the ion potential with pseudo potential. And then the plane wave ultra-soft pseudo potential method is used, with the generalized gradient functional (GGA) utilized to deal with the exchange correlation potential. Plane-wave energy cutoff 300 eV and Monkhorst–Pack *k*-point gird of $(3 \times 4 \times 1)$ were used. In addition, vacuum was entered between two surfaces of each model and the thickness is set of 8 Å to avoid the interaction. 5×2 groups were build in four crystal surfaces of CrOOH and one crystal bulk of $Cr(OH)_3$, each model have two files, before and after the O_2 adsorb at the surface. For each slabs, the bottom of atoms are fixed, allowing the Cr on the outermost relaxed to attached oxygen. The figure can be seen at Fig. 1 from (a–e).

3. Results and discussion

3.1 Characterization and analysis

The crystal structure models of β-CrOOH and $Cr(OH)_3$ were constructed and optimized was shown in Fig. 1. The chemical adsorption models of oxygen molecules on different surfaces by

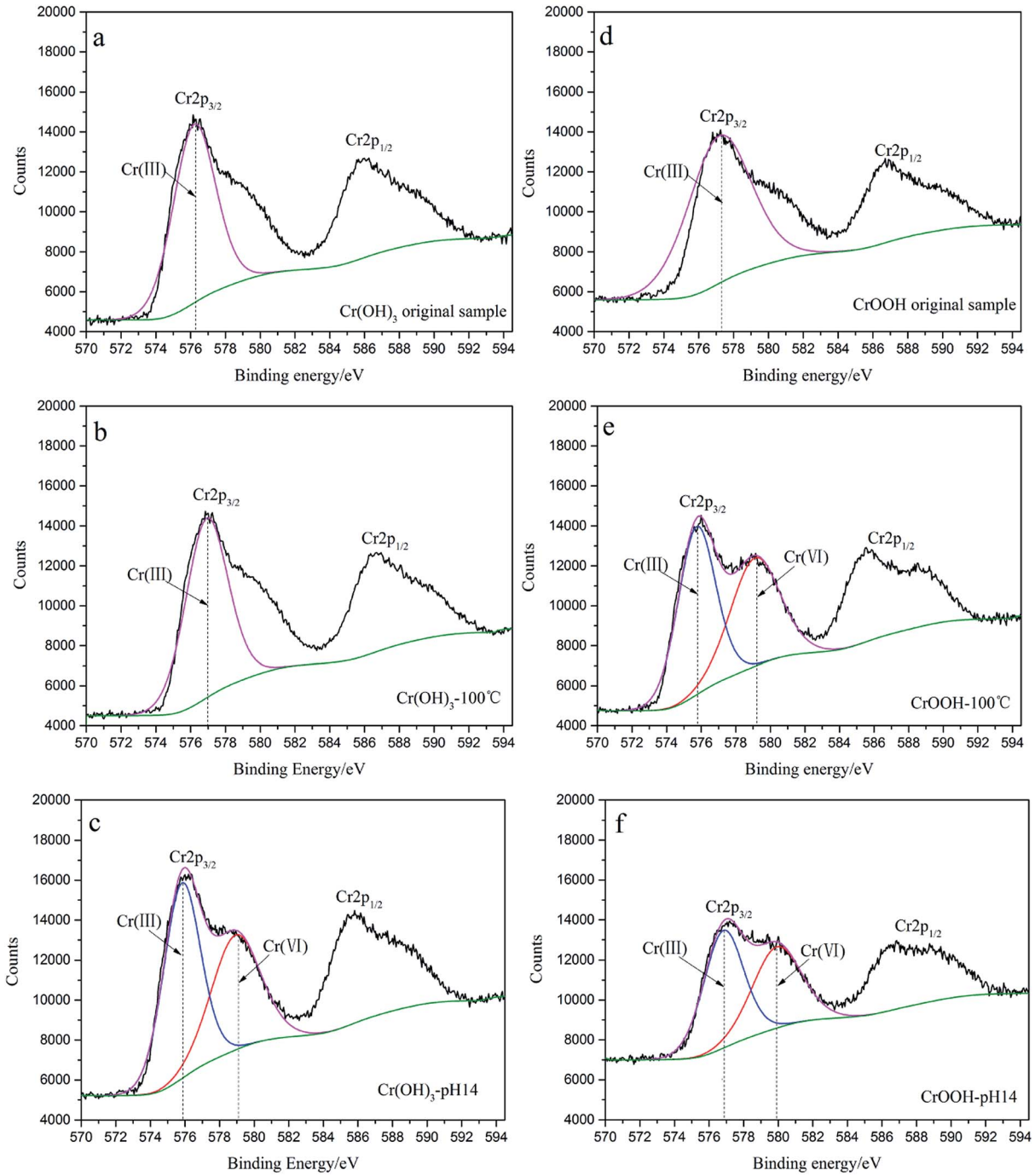

Fig. 3 (a) The original $Cr(OH)_3$ sample; (b) $Cr(OH)_3$ at 100 °C; (c) $Cr(OH)_3$ at pH = 14; (d) original CrOOH sample; (e) CrOOH at 100 °C; (f) CrOOH at pH = 14.

Table 1 Relative content of different element in different sample

Condition	Element	Relative content/%
$Cr(OH)_3$ original sample	O	85.13
	Cr	13
	Na	1.87
$Cr(OH)_3$ in 100 °C	O	85.25
	Cr	13.15
	Na	1.6
$Cr(OH)_3$ in pH 14	O	74.68
	Cr	10.87
	Na	14.45
CrOOH original sample	O	84.74
	Cr	7.44
	Na	7.83
rOOH in 100 °C	O	76.15
	Cr	10.53
	Na	13.32
CrOOH in pH 14	O	73.77
	Cr	5.17
	Na	21.06

intercepting different crystal planes of (101), (310), (321), and (110) crystal planes was constructed, relating with X-ray diffraction result. By ICSD database,[18] the crystal structure of β-CrOOH and $Cr(OH)_3$ at the very start were created and optimized. The β-CrOOH is belong to *Pnnm* space group, while $Cr(OH)_3 \cdot nH_2O$ is belong to *P*1*m*1 space group. With optimizing the crystal structure, we can get the most stable absorb model which has lowest internal energy. The figure can be seen at Fig. 10 from (a and b).

In order to obtain information about the influence of temperature and pH in the process of Cr(III) be oxidized to Cr(VI), the morphology of CrOOH and $Cr(OH)_3$ were studied before and after oxidation.

As can be seen in Fig. 2, the average particle size of $Cr(OH)_3$ has change little whether in high temperature or in extreme alkaline environment. While the CrOOH particle is visualized to have a crystallized sheet structure before oxidation. It's appeared non-crystallised lumpy aggregates after the oxidation. The floccule has larger size than the particle before oxidation, and the origin of the new structure maybe have some relation with yellow chromate.

In order to further analyze the valence state, binding form, and relative content of chromium before and after the reaction, XPS narrow-band scanning for Cr (2p) orbit has been used in our study. After peaking separations and fitting, the result can be seen from Fig. 3, and the relative content of element can be seen from Table 1.

As you can see in the Fig. 3, the Cr 2p spectra has separated into Cr $2p_{3/2}$ peak and Cr $2p_{1/2}$ peak because of spin splitting. By comparing the XPS spectra of chromium hydroxide under different conditions in Fig. 3(a–c), the Cr(VI) peak appeared within the high alkaline environment after 14 days. The binding energy is 579.05 eV which is closed to 579.8 eV of Na_2CrO_4 (the 1.3–1.4 eV fluctuation is because of the overlap with the multiplied splitting of Cr(III)). However, we can find Cr(VI) peak of hydroxy chromium both in high temperature and pH. And it has broader chemical shift between the Cr(III) to Cr(VI).

Comparing high temperatures with high pH environments From Fig. 3(e), (f), the peak fitting envelope of Cr(III) and Cr(VI) can illustrate the relative content of them. In alkaline environment, the Cr(III) is more likely to be oxidized obviously. Moreover, the Table 1 listed the relative contend of element. The content of Na increased after the oxidation of Cr(III), and the more content of Na represented the more CrO_4^{2-} has been made. So the CrOOH which exposed to air in alkaline environment seemed to more lively in all of the sample.

3.2 Cr(III) reoxidation experiment and analysis of chemical reaction dynamics

To explore the effects of temperature and pH on Cr(III) reoxidation, we measured the concentration of Cr(VI) by spectrometer. The Fig. 4 has showed the rule of Cr(III) oxidation with the effect of pH. As the pH increased, the Cr(VI) content in the CrOOH and $Cr(OH)_3$ samples increased, while $Cr(OH)_3$ does not occur oxidation under pH of 10. In addition, as time goes on,

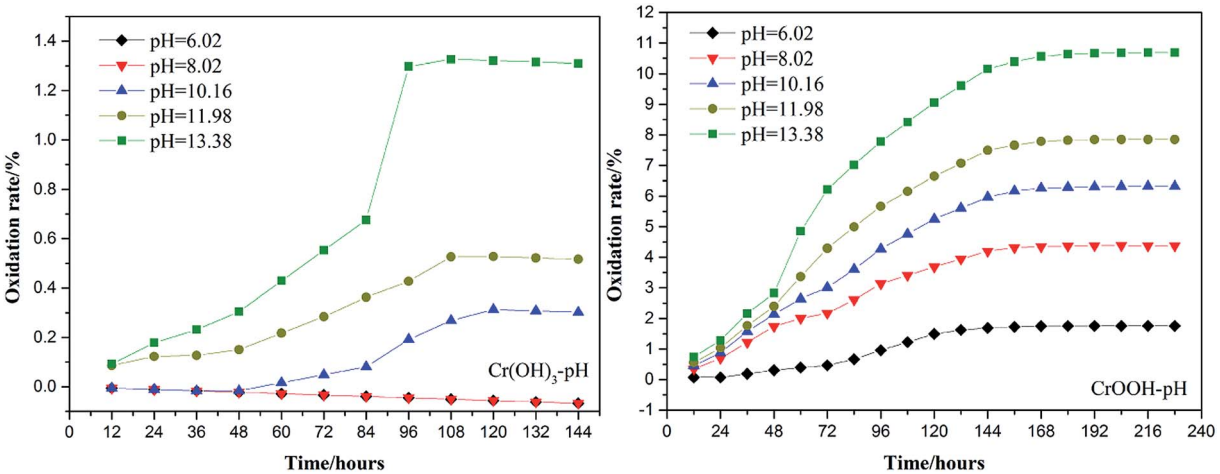

Fig. 4 The effect of pH value in the process of Cr(III) oxidation.

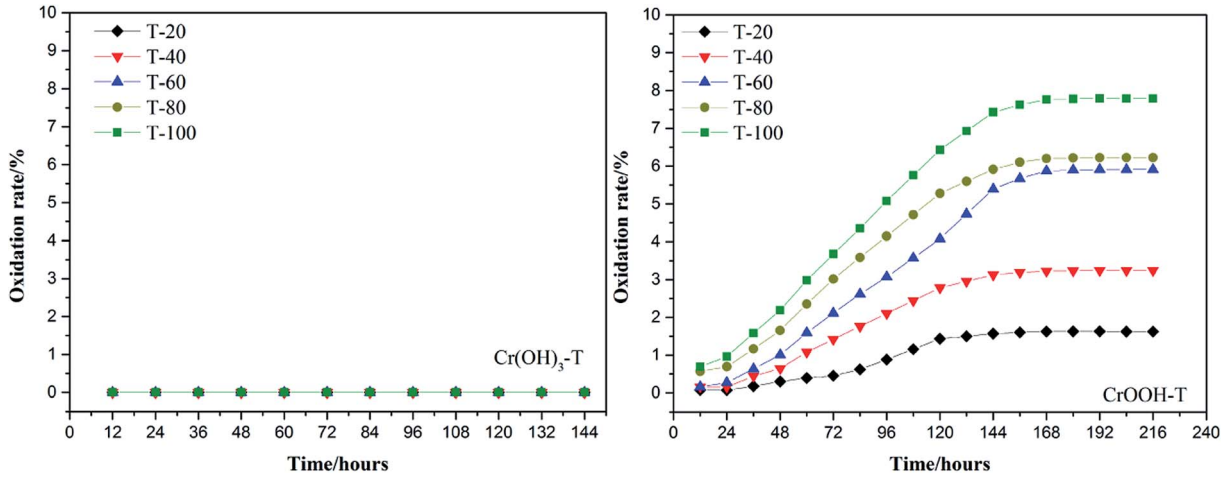

Fig. 5 The effect of temperature in the process of Cr(III) oxidation.

the reaction becomes closer to equilibrium, and CrOOH occurs longer than $Cr(OH)_3$ in the oxidation process. As regards to the rule of Cr(III) oxidation with the effect of temperature, which can be seen in Fig. 5. $Cr(OH)_3$ did not reoxidize with the increase of temperature. According to the previous thermodynamic analysis, $Cr(OH)_3$ is not easy to be oxidized at lower pH, even at high temperature. But the Cr(VI) in CrOOH sample increases as the temperature rises. The oxidation rate is lower than the CrOOH in higher pH, which illustrates pH seemed has more effect on oxidation process than temperature.

To make a deep understanding of the oxidation process from Cr(III) to Cr(VI), we have a dynamic fitting of the results on the reoxidation part. First, the effect of pH in the process can be seen in Fig. 6. Combining the results of the kinetic constant K values in Table 2, we find that the chemical reaction rate constant K increases as pH and temperature rise up. Through previous thermodynamic analysis, increased concentration of OH^- reduces Gibbs free energy for reoxidation reaction of Cr(III). And the rate constant of CrOOH is one magnitude larger than the $Cr(OH)_3$. Moreover, by fitting the Arrhenius equation of temperature and chemical reaction rate constants, the $1/T - \ln K$ has linear relationship as can be seen in Fig. 7, and the rate constant of CrOOH with different temperature is closed to the constant with different pH except pH = 14. Although the CrOOH in higher pH can be oxidated easier, the production of sodium hydroxide helps make reoxidation of Cr(III) easier within high temperature. Plus, molecular kinetic energy increases as

Table 2 Kinetic constant K in oxidation reaction with different pH

Sample	pH	K (25 °C)/mol L^{-1} h^{-1}	R (fitting variance)
$Cr(OH)_3$	10	2.74×10^{-5}	0.8737
	12.04	4.57×10^{-5}	0.9323
	13.86	1.32×10^{-4}	0.8529
	6.02	1.31×10^{-4}	0.9555
	8.02	2.75×10^{-4}	0.9761
CrOOH	10.16	4.11×10^{-4}	0.9847
	11.98	5.25×10^{-4}	0.9691
	13.38	7.35×10^{-4}	0.9565

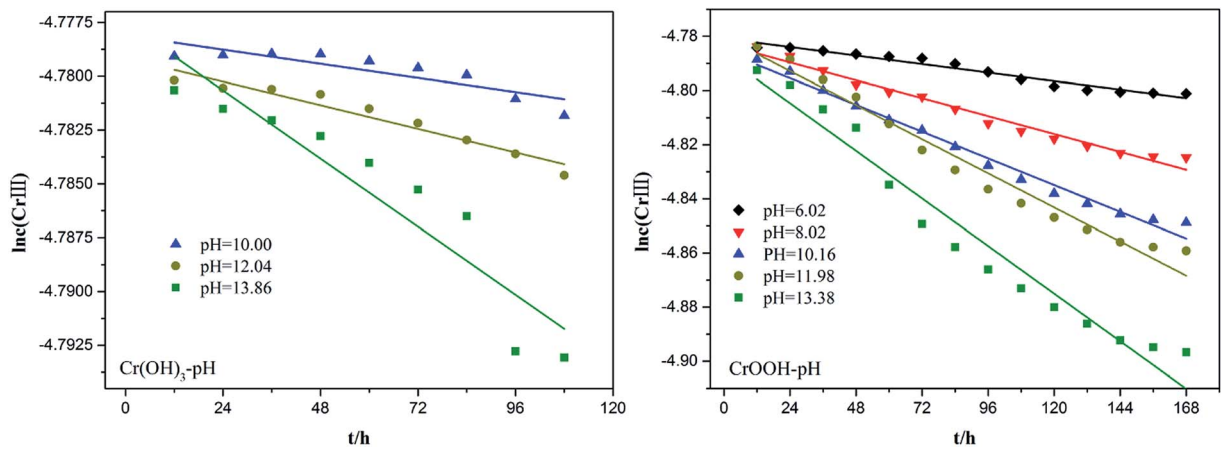

Fig. 6 Kinetic fitting results of the oxidation reaction of Cr(III) in different pH.

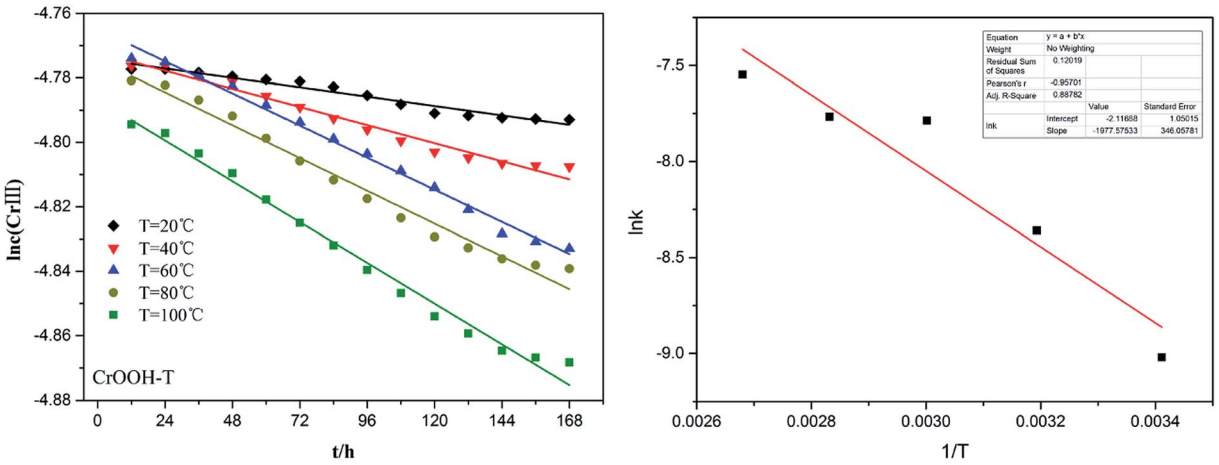

Fig. 7 Kinetic fitting results of the oxidation reaction of Cr(III) in different temperature.

the temperature rises, which greatly contribute to reaction (Table 3).

3.3 Potential-PH diagrams of Cr(III)–H_2O system at different ionic activity

All of the data we used in this part of thermodynamic calculation are obtained from ref. 19 and 20. By calculating Gibbs free energy of $Cr(OH)_3$ and CrOOH oxidation reaction, we can evaluate the difficulty of the chemical reaction. The chemical reactions are as follows:

$$CrO_{4(aq)}{}^{2-} + 5H_{(aq)}{}^{+} + 3e^{-} \overset{OH^-}{\leftrightarrow} Cr(OH)_{3(aq)} + H_2O_{(l)}$$

$$CrO_{4(aq)}{}^{2-} + 5H_{(aq)}{}^{+} + 3e^{-} \overset{OH^-}{\leftrightarrow} CrOOH_{(aq)} + 2H_2O_{(l)}$$

So, the Nernst equation of the reactions can be listed as bellows:

$$E_T = E_T^{\Theta} - (5 \times 2.303RT/3F)\mathrm{pH} + (2.303RT/3F)\lg a_{CrO_4{}^{2-}} \Big/ a_{Cr(OH)_3}$$

$$E_T = E_T^{\Theta} - (5 \times 2.303RT/3F)\mathrm{pH} + (2.303RT/3F)\lg a_{CrO_4{}^{2-}} \Big/ a_{CrOOH}$$

Table 3 Kinetic constant K in oxidation reaction with different temperature

Sample	T/K	K (pH = 6)/mol L^{-1} h^{-1}	R (fitting variance)
CrOOH	293.15	1.21×10^{-4}	0.9537
	313.15	2.34×10^{-4}	0.9727
	333.15	4.15×10^{-4}	0.9864
	353.15	4.24×10^{-4}	0.9909
	373.15	5.27×10^{-4}	0.9794

After Cr(VI) is reduced to Cr(III), lime is added to neutralize to neutral or alkaline. Cr(III) combines with OH^- to form $Cr(OH)_3$ or transforms to CrOOH precipitation, $Cr(OH)_3$ and CrOOH are oxidized to hexavalent chromium by oxygen in air under alkaline conditions. As the reaction are happened in alkaline environment, the standard electromotive force of the primitive cell can be converted to the change of standard Gibbs free energy value. So the final reaction equation and Gibbs free energy equation is as follows:

$$Cr(OH)_3 + 5OH^- = CrO_4{}^{2-} + 4H_2O + 3e^-$$

$$\Delta G_1 = \Delta G_1^{\Theta} + 2.303RT \lg a_{CrO_4{}^{2-}} + 11.515RT \lg OH^-$$

$$\Delta G_1 = 430.07 + 5.71 \lg a_{CrO_4{}^{2-}} - 28.54\ \mathrm{pH\ kJ\ mol^{-1}}$$

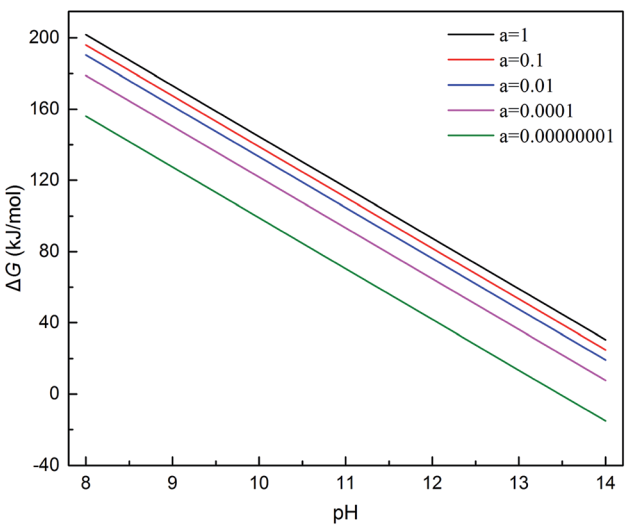

Fig. 8 Gibbs free energy of $Cr(OH)_3$ oxidation (reaction 1).

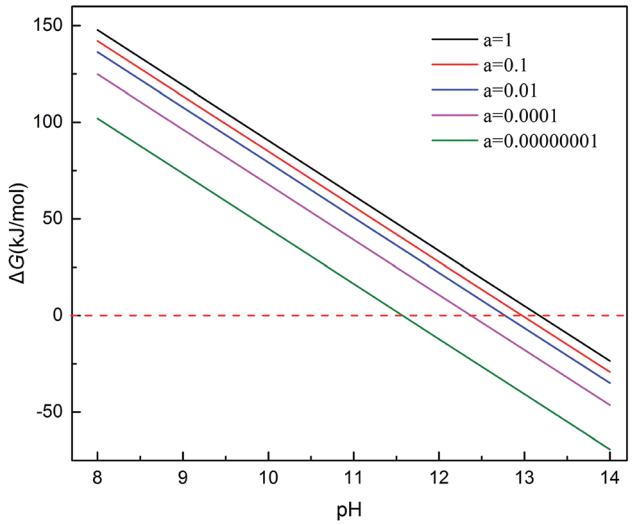

Fig. 9 Gibbs free energy of CrOOH oxidation (reaction 2).

If the activity of $a_{CrO_4^{2-}} = 1,$, $\Delta G_1 = 430.07 - 28.54$ pH kJ mol^{-1}, the pH–ΔG diagram with different $a_{CrO_4^{2-}}$ can be seen at Fig. 8.

While, as the CrOOH are oxidized to hexavalent chromium by oxygen in air under alkaline conditions. The reaction equation is as follows:

$$CrOOH + 5OH^- = CrO_4^{2-} + 3H_2O + e^-$$

$$\Delta G_2 = \Delta G_2^{\ominus} + 2.303RT \lg aa_{CrO_4^{2-}} + 11.515RT \lg OH^-$$

$$\Delta G_2 = 375.98 + 5.71 \lg a_{CrO_4^{2-}} - 28.54 \text{ pH kJ mol}^{-1}$$

If the activity of $a_{CrO_4^{2-}} = 1$, 0.1, 0.01, 0.0001, 0.00000001, the pH–ΔG diagram with different $a_{CrO_4^{2-}}$ can be seen at Fig. 9.

Through the pH–ΔG diagram, the principle effects of pH within certain ionic activities of each reaction can be summarized as below: (a) as the $a_{CrO_4^{2-}}$ is lower, both the diagram of $Cr(OH)_3$ and CrOOH will decline. It means the lower activity of CrO_4^{2-} will correspond to lower equilibrium potential, promoting the CrO_4^{2-} reduced to $Cr(OH)_3$ or CrOOH; (b) the higher temperature will also decline the diagram of $Cr(OH)_3$ and CrOOH, due to the Nernst equation; (c) in higher pH region, the negative energy potential illustrate both the $Cr(OH)_3$ and CrOOH has the possibility to convert to CrO_4^{2-}; (d) $Cr(OH)_3$ required higher pH than CrOOH as oxidized to CrO_4^{2-}.

3.4 Crystal structure analysis of trivalent chromium compound

3.4.1 Chemical adsorption analysis. The oxidation of trivalent chromium in soil by oxygen in air is a process of chemical adsorption. The oxygen absorb in CrOOH or $Cr(OH)_3 \cdot nH_2O$ molecular surface selectively, inducing the solid molecular lose the electrons. So the negative ions absorb on the surface of positively charged solids ultimately and become Cr–O chemical bond. To study this chemical adsorption process, (101), (110), (310), (321) crystal surface of β-CrOOH were selected as adsorb model.

After cleaving the surface of crystal structure, an vacuum space between two layers of atoms was slabbed, in order to input the oxygen between the surfaces. With relaxing the other atoms except the outermost Cr atom, we can simplify the operation process and ensure the optimal model. After optimization, the stable adsorption model of CrOOH and $Cr(OH)_3 \cdot nH_2O$ can be used to do the next work. The oxygen molecular was input to finalize our computation of electronic density of states through the process. And the solid model adsorb energy is defined as:

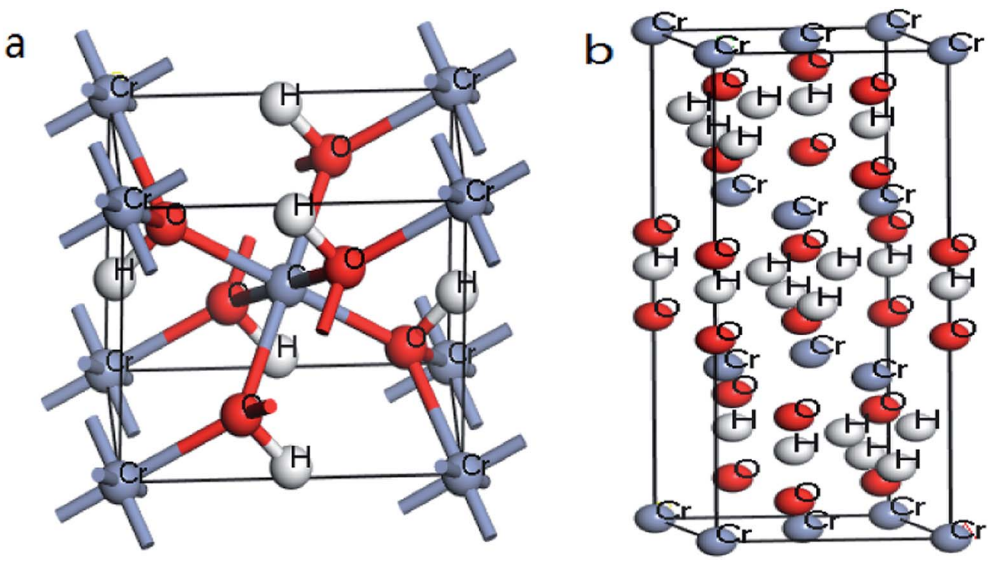

Fig. 10 (a) Optimized structures of β-CrOOH in *Pnnm* space group; (b) $Cr(OH)_3.nH_2O$ in *P*1*m*1 space group.

Table 4 The energy of O_2, optimized model of CrOOH or $Cr(OH)_3$, adsorption model of CrOOH or $Cr(OH)_3$, and the adsorb energy are listed below

Surface	$E(O_2)$/eV	E(OPT model)/eV	E(adsorption model)/eV	ΔQ/eV
(101)	−867.78	−6708.15	−7579.32	−3.39
(110)	−867.78	−6742.18	−7610.28	−0.32
(310)	−867.78	−6707.03	−7577.81	−3
(321)	−867.78	−6703.5	−7574.21	−2.93
$Cr(OH)_3$ bulk	−867.78	−20250.68	−21131.65	−13.19

Table 5 The distance of Cr–O chemistry bonds which are optimized in the adsorption model are also listed

Adsorption surface	Cr–O/Å	O–O/Å
(101)	1.689	1.313
(110)	4.11	1.26
(310)	1.702	1.289
(321)	1.679	1.288
$Cr(OH)_3$	1.747	1.316

$$E_{ad(Cr^{3+}\ solid\ molecular)} = -[E_{(O_2/Cr^{3+}\ solid\ surface)} - E_{(Cr^{3+}\ solid\ surface)} - E_{(O_2)}]/N_{first\ Cr^{3+}\ atom}$$

E_x means crystal internal energy, while N means the number of atoms which are connect to the oxygen molecular. The calculated data is put in Table 4. It can be seen that the CrOOH (101) surface require more adsorb energy than the other three surface of the CrOOH. While the (110) surface of CrOOH need relatively few energy than the other crystal surface. Moreover, the $Cr(OH)_3$ structure has the most adsorb energy in all of computational model, reflecting the difficulties of chemical adsorption is higher than CrOOH model.

Through the bond distance which can be seen at Table 5, the stability of the optimized adsorption structure and the energy consumed by bonding can be reflected. In the surface of CrOOH, the (101) lattice plane has the shortest Cr–O chemistry bond with 1.689 Å, while $Cr(OH)_3$ surface has longer Cr–O bond than the most cleaved surface of CrOOH. However, (110) surface of CrOOH has Cr–O bond of 4.16 Å which is greater than the length of the molecule van der Waals force described in the literature (3 Å),[21] which indicates that the chromium atom on the crystal plane is less likely to be bound to the oxygen atom to form a covalent bond or electrovalent bond (and the lowest adsorb energy has well illustrated this weak interaction). Besides, the distance of O–O bonds from (101), (310), (321) surface and $Cr(OH)_3$ model is higher than 1.26 Å, but lower than 1.49 Å (this two figures are the distance of O_2^- and O_2^{2-}, computing by the MO theory),[22,23] showing the atom of O are quiet possible combined with Cr in covalent bond with different electronic proportions.

Subsequently, the electron translation can be analyzed with the figure of electron density and differential charge density. The figure can be seen at Fig. 11 from (a and b).

It's clear to view the accumulation or depletion of electron within the optimize adsorption structure by the Fig. 11b (O_2 adsorption on other systems is similar and thus not shown). The charge density difference is defined as:[24] $\rho(O_2/Cr) - \rho(O_2) - \rho(Cr)$, where $\rho(O_2/Cr)$, $\rho(O_2)$, and $\rho(Cr)$ are the total charge densities of O_2/Cr, a free O_2 molecule, and Cr systems without changing their atomic positions. Most of the electron are accumulatd around O_2, while the red area indicate the electron depletion of Cr, showing in the Fig. 11b. It is obvious that upon adsorption electrons accumulate on the O_2 $2\pi^*$ orbitals. The electron density on Cr is highly polarized to maximize the electrostatic interaction between the negative O_2 and the Cr cationic. In contrast, the deformation charge density of (110) surface, showing the independency electron cloud of Cr and O_2. The non-electron cloud overlap indirectly illustrates the difficulty of forming a Cr–O covalent bond on the (110) crystal plane.

In order to best understand the nature of chemical adsorption and interatomic bonding theory, the DOS of each surface of CrOOH and $Cr(OH)_3$ before and after adsorption of oxygen was calculated. The DOS can reflect the electronic states within the unit energy interval, as well as the PDOS can illustrate the way that the total energy separated in each electronic orbit.[25]

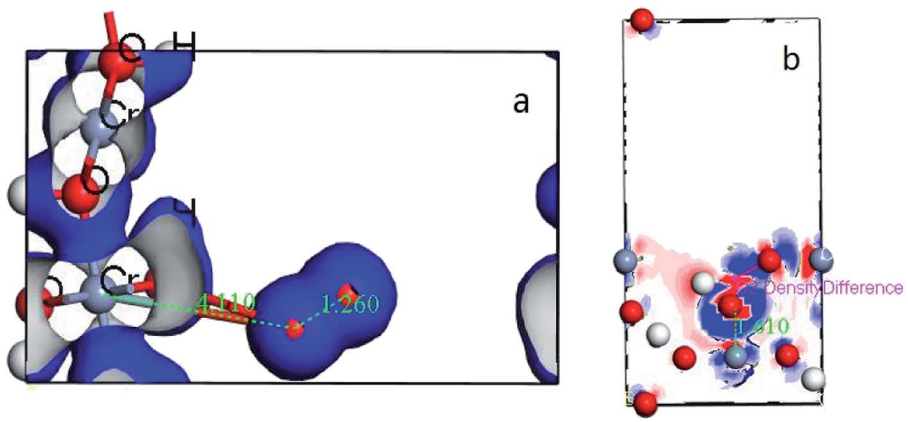

Fig. 11 (a) the deformation charge density of (110) surface; (b) difference charge density of CrOOH (101) surface.

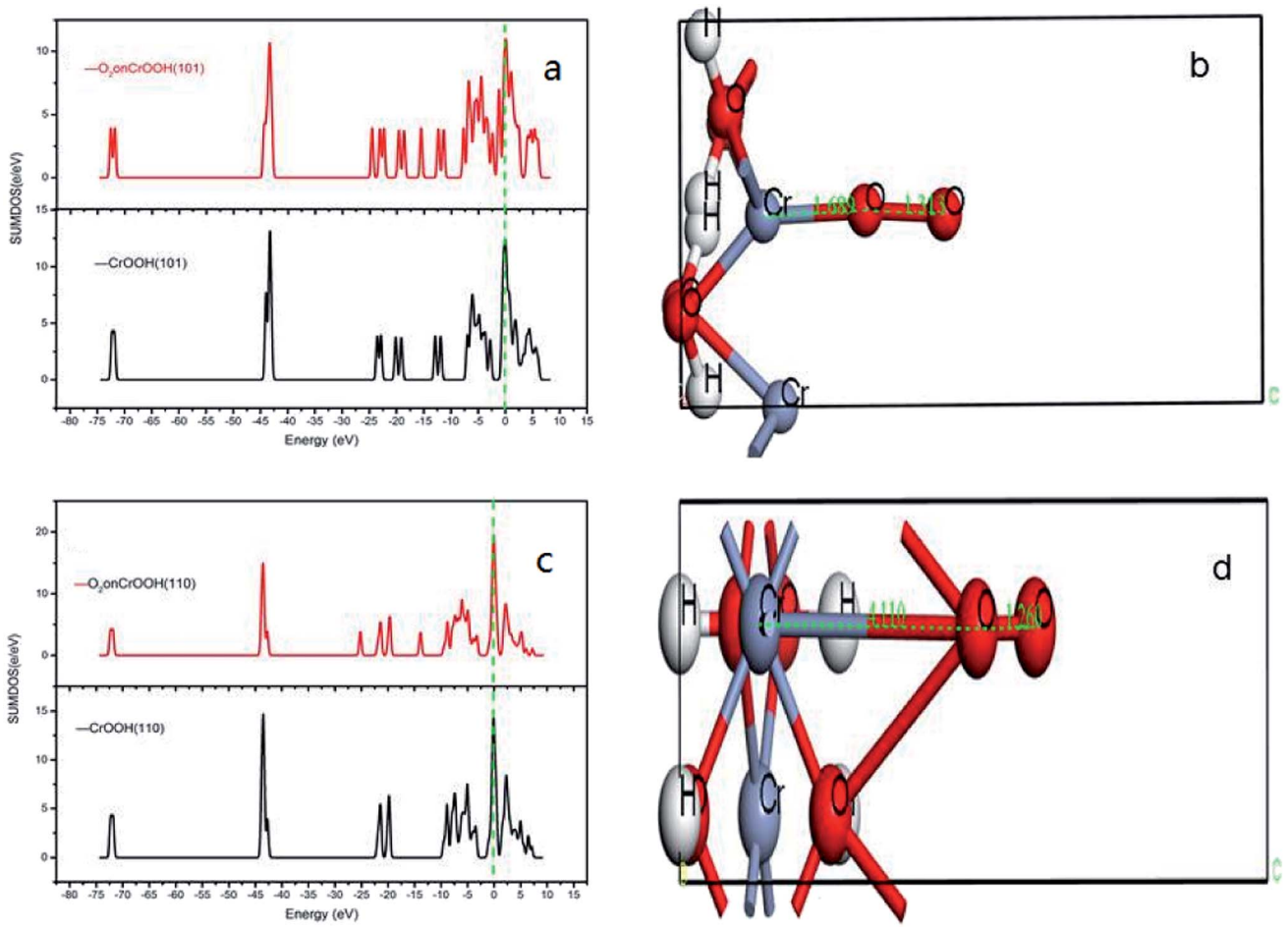

Fig. 12 (a) the total density of states of CrOOH (101) surface adsorption model; (b) the side view of optimized CrOOH (101) surface adsorption model; (c) the total density of states of CrOOH (110) surface adsorption model; (d) the side view of optimized CrOOH (110) surface adsorption model.

It can be vividly seen at the Fig. 12–14, that the total density of states of four kinds of crystal surface change before and after the oxygen molecule adsorb at four crystal surface. The electron on the surface of the crystal translates to the low energy level, and the surface energy decreases. At (101) surface, most of the electrons of −42 eV transition to the −18 eV and much lower energy level closed to the Fermi energy surface (the larger integral peak area close to Fermi surface indicates that more electrons gather around it). A little change at the (110) surface, showing a small amount of electrons aggregate at −18 eV and −12 eV. While at (310) surface, the electron transition from −45 eV to −15 eV and −8 eV in the distribution of electronic state density of chromium hydroxyl oxide on crystal plane after adsorption, and the electron transition from −45 eV to −8 eV and −5 eV at the (321) surface after the adsorption. However, the surface state density of chromium hydroxide with optimized structure is −73 eV, 43 eV, 20 eV, closely equal to the electronic state density of chromium hydroxide adsorbed on O_2, which distributes at −73 eV, 43 eV and 18 eV. So, there is no obvious change in the density of electronic states of chromium hydroxide adsorbed on O_2.

In addition, the relationship between oxide structure and newly formed covalent bond can be found by PDOS (projected density of states) which can be seen at the Fig. 15 and 16. Usually, there are three bonding principle to construct molecular orbital (MO) by atom orbital (AO):[26] (1) symmetry matching; (2) closely energy level; (3) maximum overlap of atom orbital. In this paper, we calculate the PDOS of O_2 on CrOOH (101) surface and O_2 on $Cr(OH)_3$ adsorption model. By Fig. 15, distributing the energy of O_2 into three main regions:[27] (a) O_2-bonding region of σ and π^*_{2p} orbital (−7.5 eV to −3 eV); (b) O_2-antibonding region of π^*_{2p} orbital (−2.5 eV to 0.5 eV); (c) σ^*_{2p} and π^*_{2p}- antibonding region (0.5 eV to 5 eV). While, the individual O_2 atom states of $Cr(OH)_3$ is more narrow than CrOOH model. The resonance peaks of CrOOH and O_2 model is concentrate on (−5 eV to −3 eV) closed to Fermi surface (from O_2 (s) orbital collaborating with Cr (d) orbital), and the resonance peaks of $Cr(OH)_3$ and O_2 model is overlapped in (−7.5 eV to −5 eV) far away from Fermi surface illustrating more bonding energy than CrOOH.

In adsorption process, adsorption electrons has accumulated on the O_2 2π* orbitals.[28] The highly density of electrons on Cr is polarized to maximize the electron interaction between the negative O_2 and Cr interaction. With a few resonance peaks

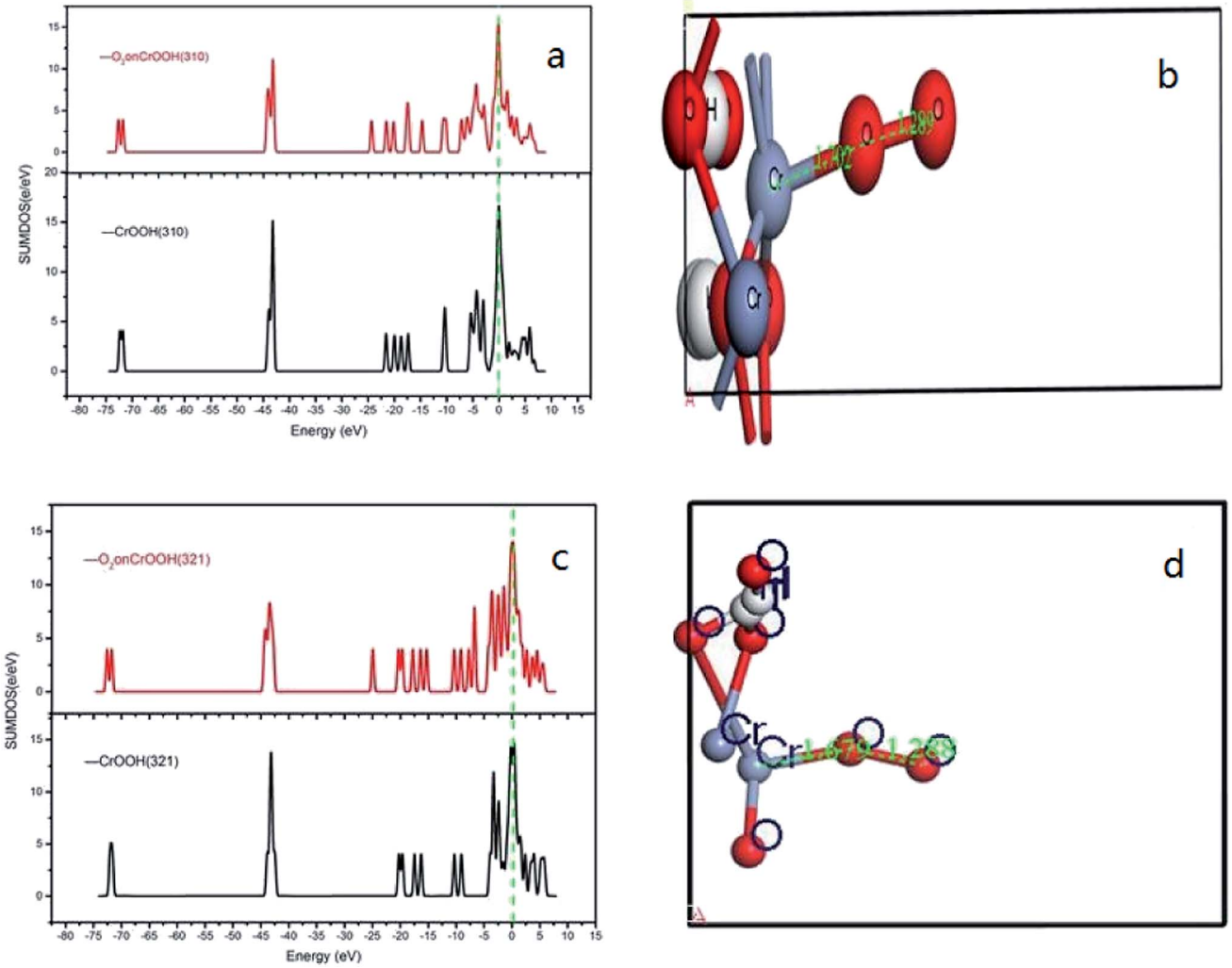

Fig. 13 (a) the total density of states of CrOOH (310) surface adsorption model; (b) the side view of optimized CrOOH (310) surface adsorption model; (c) the total density of states of CrOOH (321) surface adsorption model; (d) the side view of optimized CrOOH (321) surface adsorption model.

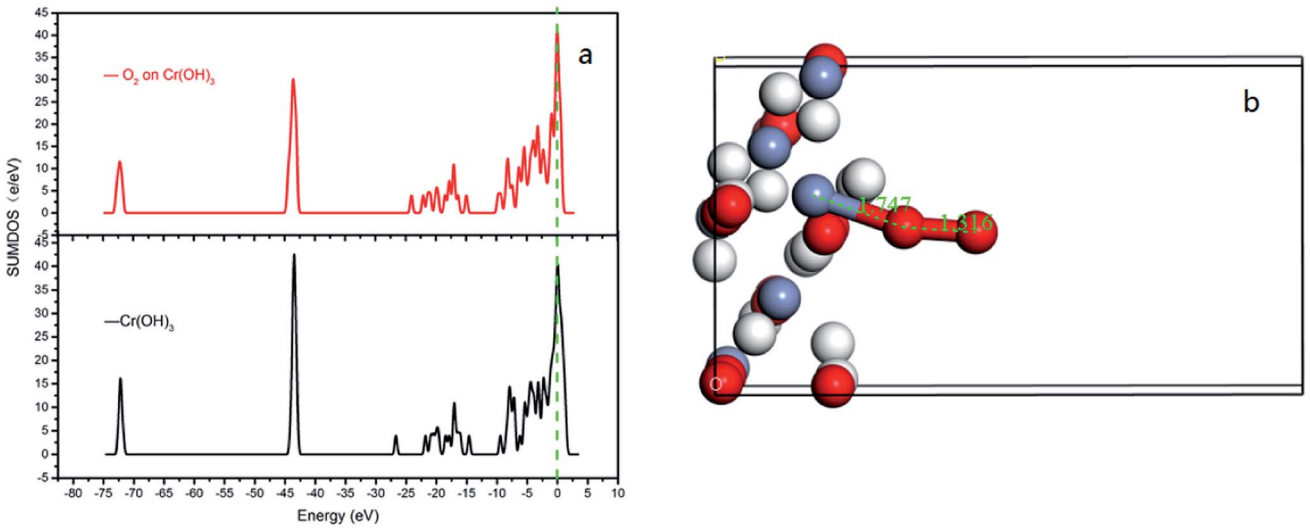

Fig. 14 (a) the total density of states of $Cr(OH)_3$ bulk adsorption model; (b) the side view of optimized $Cr(OH)_3$ bulk adsorption model.

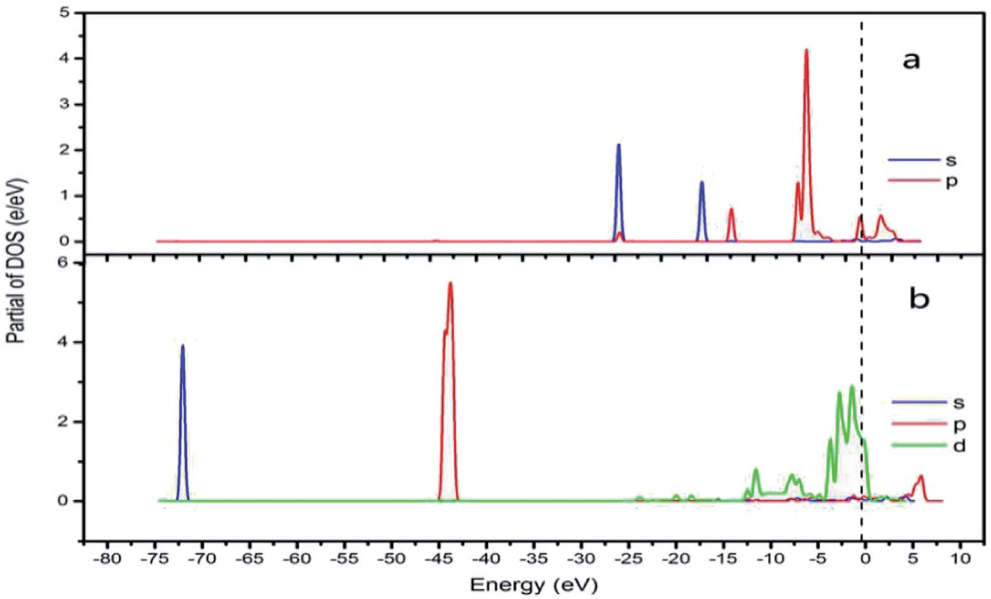

Fig. 15 CrOOH (101) surface PDOS (a) O_2 PDOS of s and p orbital; (b) Cr PDOS of s, p and d orbital).

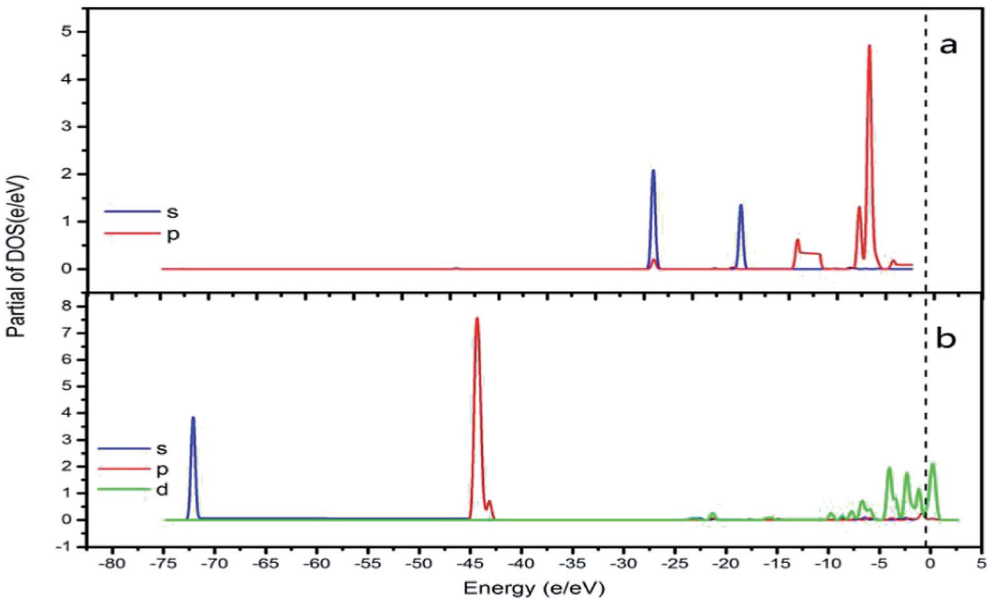

Fig. 16 $Cr(OH)_3$ surface PDOS (a) O_2 PDOS of s and p orbital; (b) Cr PDOS of s, p and d orbital.

around Fermi level, which are found to be the mixing states between the d-Cr-O_2 model and the O_2 π^*_{2p} orbitals, we can see the d(Cr)–O_2 π^*_{2p} mixing orbitals possesses clear covalent bonding characteristics between $Cr(OH)_3$/CrOOH and O_2.

Furthermore, the empty d-states of the Cr (−5 eV of CrOOH surface and $Cr(OH)_3$) is mixing with O_2 π^*_{2p} orbitals, which further lower the O_2 π^*_{2p} orbitals energy level and improve the stability of adsorption process.

4. Conclusion

(1) Based on the reoxidation experiment and chemical kinetic analyze of Cr(III). The oxidation rate of Cr(III) in air without MnO_2 and H_2O_2 was studied. As setting the reductive sample within different pH and temperature, both the CrOOH and $Cr(OH)_3$ has the potential to be oxidized in wet alkaline environment while remain stable in neutral or acid condition. In addition, the chemical reaction equilibrium constant K of CrOOH is higher than $Cr(OH)_3$. Besides, the SEM and XPS result of Cr(III) has illustrated that the CrOOH is more easily to be oxidized than $Cr(OH)_3$.

(2) Based on the thermodynamic computation, the pH–ΔG diagram of 298 K with certain ionic activity has showing the principle in oxidized reaction of CrOOH and $Cr(OH)_3$. Both CrOOH and $Cr(OH)_3$ can convert to CrO_4^{2-} under alkaline environment, but CrOOH has more potential to be oxidized to

CrO_4^{2-} in pH (11.5–14). However, the $Cr(OH)_3$ are more stable, and they have difficulty with oxidizing to CrO_4^{2-} except in the pH (14) with lower CrO_4^{2-} activity of 0.00000001.

(3) By using DFT method, we has constructed different crystal model of CrOOH and $Cr(OH)_3$. Comparing with the adsorption energy and Cr–O bond, CrOOH are prone to react with oxygen than $Cr(OH)_3$. While the distance between Cr and O in (110) adsorption surface is over 3 Å, which is more likely to occur a van der Waals' interaction. Moreover, the DOS and PDOS diagram illustrate the Cr–O covalent bond has been made through the process of adsorption, and the resonance peak of Cr and O atom closed to Fermi energy, vividly showing the mixing orbitals of Cr (d) and O_2 (π^*_{2p}) has been made through the reaction between Cr(III) and oxygen.

Conflicts of interest

There are no conflicts to declare.

Acknowledgements

This work was financially supported by the National Key R&D Program of China (Grant No. SQ2018YFC180012).

Notes and references

1 D. J. Paustenbach, B. L. Finley, F. S. Mowat and B. D. Kerger, *J. Toxicol. Environ. Health, Part A*, 2003, **66**(14), 1295–1339.
2 K. Kitagishi and I. Yamane, *J. Environ. Qual.*, 1981, **12**, 426.
3 I. Aharchaou, M. Rosabal, F. Liu, E. Battaglia and C. Fortin, *Aquat. Toxicol.*, 2016, **182**, 49.
4 A. Davis and R. L. Olsen, *Groundwater*, 2010, **33**, 759–768.
5 J. S. Geelhoed, J. C. L. Meeussen, D. G. Lumsdon, S. Hillier, M. J. Roe, R. P. Thomas, R. J. F. Bewley, J. G. Farmer and E. Paterson, *Environ. Geochem. Health*, 2001, **23**, 261–265.
6 R. R. Patterson and S. Fendorf, *J. Environ. Sci. Technol.*, 1997, **31**, 2039–2044.
7 M. Pettine, F. J. Millero and R. Passino, *Mar. Chem.*, 1994, **46**, 335–344.
8 C. Kim, Q. Zhou, B. Deng, E. C. Thornton and H. Xu, *Environ. Sci. Technol.*, 2001, **35**, 2219–2225.
9 C. Kim, Y. Lan and B. Deng, *Geochem. J.*, 2007, **41**(6), 397–405.
10 A. R. Wadhawan, A. T. Stone and E. J. Bouwer, *Environ. Sci. Technol.*, 2013, **47**, 130724102802006.
11 C. Oze, D. K. Bird and S. Fendorf, *Proc. Natl. Acad. Sci. U. S. A.*, 2007, **104**(16), 6544–6549.
12 M. Chrysochoou, D. R. Ferreira and C. P. Johnston, *J. Hazard. Mater.*, 2010, **179**, 650–657.
13 Z. Zhang, L. Rao, D. Rai and S. B. Clark, *MRS Online Proc. Libr.*, 2004, **824**, CC6.5.
14 F. Dik, J. Farid, M. Guillaume, O. Luca, C. Andrea, S. M. Webb, A. Jean-Paul, F. Emmanuel, G. Fran?Ois and G. E. Brown, *Environ. Sci. Technol.*, 2009, **43**, 7384–7390.
15 N. Miyata, Y. Tani, M. Sakata and K. Iwahori, *J. Biosci. Bioeng.*, 2007, **104**, 1–8.
16 R. Serramaia, M. Bellier, S. Chastka, K. Tranhuu, A. Subowo, J. D. Rimstidt, P. M. Usov, A. J. Morris and F. M. Michel, *ACS Appl. Mater. Interfaces*, 2018, **10**, 21224–21234.
17 A. D. Bokare and W. Choi, *J. Hazard. Mater.*, 2014, **275**, 121–135.
18 R. Allmann and R. Hinek, *Acta Crystallogr.*, 2010, **63**, 412–417.
19 J. Gmehling, *Chem. Ing. Tech.*, 1978, **50**, 933.
20 M. Selleby, M. Hillert and J. Ågren, *CALPHAD: Comput. Coupling Phase Diagrams Thermochem.*, 2011, **35**, 342–345.
21 I. E. Dzyaloshinskii, E. M. Lifshitz and L. P. Pitaevskii, *Adv. Phys.*, 1961, **10**, 165–209.
22 D. Rabinovich, *J. Chem. Educ.*, 2003, **80**, 1015–1020.
23 D. Tudela and V. Fernández, *J. Chem. Educ.*, 2003, **80**, 1381.
24 H. Fukuyama, *Phys. Rev. B: Solid State*, 1978, **17**, 535–541.
25 S. Chrétien and H. Metiu, *J. Chem. Phys.*, 2008, **129**, 074705.
26 I. N. Levine, *Quantum Chemistry: International Edition*, Pearson Schweiz Ag, 2013.
27 M. D. Johannes, S. L. Karen and T. L. Corey, *Solid State Ionics*, 2016, 83–89.
28 A. Kistanov, Y. Cai, D. Kripalani, K. Zhou, S. Dmitriev and Y. W. Zhang, *J. Mater. Chem. C*, 2018, 4308–4317.